



## Enhanced osteogenic activity with boron-doped nanohydroxyapatite-loaded poly(butylene adipate-co-terephthalate) fibrous 3D matrix

Aysu Arslan, Soner Çakmak & Menemşe Gümüşdereliolu


To cite this article: Aysu Arslan, Soner Çakmak & Menemşe Gümüşdereliolu (2018) Enhanced osteogenic activity with boron-doped nanohydroxyapatite-loaded poly(butylene adipate-co-terephthalate) fibrous 3D matrix, *Artificial Cells, Nanomedicine, and Biotechnology*, 46:sup2, 790-799, DOI: [10.1080/21691401.2018.1470522](https://doi.org/10.1080/21691401.2018.1470522)

To link to this article: <https://doi.org/10.1080/21691401.2018.1470522>

 View supplementary material [↗](#)

 Published online: 11 May 2018.

 Submit your article to this journal [↗](#)

 Article views: 495

 View related articles [↗](#)

 View Crossmark data [↗](#)

 Citing articles: 4 View citing articles [↗](#)



## Enhanced osteogenic activity with boron-doped nanohydroxyapatite-loaded poly(butylene adipate-co-terephthalate) fibrous 3D matrix

Aysu Arslan<sup>a</sup>, Soner Çakmak<sup>b</sup> and Menemşe Gümüşderelioğlu<sup>a</sup>

<sup>a</sup>Department of Chemical Engineering, Hacettepe University, Ankara, Turkey; <sup>b</sup>Department of Environmental Engineering, Hacettepe University, Ankara, Turkey

### ABSTRACT

In this study, three dimensional (3D) poly(butylene adipate-co-terephthalate) (PBAT) fibrous scaffolds with more than 90% porosity were fabricated via wet electrospinning method. Amorphous hydroxyapatite (HAp) and boron (B) doped hydroxyapatite (B-HAp) nanoparticles were produced by microwave-assisted biomimetic precipitation and encapsulated into PBAT fibres with the ratio of 5% (w/w) in order to enhance osteogenic activity of the scaffolds. Cell culture studies were carried out with human bone marrow derived stem cells (hBMSCs) and they showed that alkaline phosphatase (ALP) activity and the amounts of collagen and calcium were higher on B containing PBAT (B-HAP-PBAT) scaffolds during the 28-day culture period than that of the PBAT scaffolds. Moreover, hBMSCs cultivated on B-HAP-PBAT scaffolds showed significantly higher expression levels of both early and late stage osteogenic genes e.g. ALP, collagen I (COL-I), osteocalcin (OCN) and osteopontin (OPN) at day 28 than that of the PBAT scaffolds. Scanning electron microscope (SEM) photographs and energy dispersive X-ray (EDX) analysis indicated that hBMSCs produced high amounts of mineralized extracellular matrix (ECM) mainly on the surface of the 3D matrices. This study demonstrates that boron-containing 3D nanofibrous PBAT scaffolds with their osteoinductive and osteoconductive properties can be used as alternative constructs for bone tissue engineering.

### ARTICLE HISTORY

Received 19 January 2018  
Revised 22 April 2018  
Accepted 23 April 2018

### KEYWORDS

Poly(butylene adipate-co-terephthalate); wet electrospinning; boron; hydroxyapatite; bone scaffold

### Introduction

Poly(butylene adipate-co-terephthalate) (PBAT) is an aliphatic-aromatic co-polyester with high mechanical strength and excellent biodegradability. Moreover, recent studies have shown that it is biocompatible with many cell types. This property makes PBAT a promising synthetic polymeric biomaterial for tissue engineering applications [1–6]. Although synthetic biodegradable polymers have many advantages in terms of mechanical properties such as controlled biodegradation rate and processability into various functional shapes, they are lack of biological signals that limit their cell promotion [7]. Fabrication of polymer-bioactive ceramic composites is a good alternative to produce scaffolds with enhanced bioactivity and mineralization for bone tissue engineering [8].

Hydroxyapatite (HAp) is a major component of the calcified tissues and it is one of the most commonly used bioceramics for composite bone scaffold fabrication due to its osteoinductive and osteoconductive properties [9–11]. Substitution of ions into the structure of HAp enhances its osteoinductive capacity. Since inorganic component of the natural bone primarily consists of HAp with trace amounts of ions such as Na<sup>+</sup>, CO<sub>3</sub><sup>2-</sup>, Mg<sup>2+</sup>, K<sup>+</sup>, F<sup>-</sup>, etc., ion-doped HAp facilitate bone regeneration due to their enhanced osteoconductive properties [12,13]. In a recent study, our research

group successfully synthesized boron-doped HAp (B-HAP) via microwave-assisted biomimetic precipitation method and observed that addition of B remarkably enhanced the osteoinductive effect of HAp [14].

In many studies, electrospun fibres that containing nano- or micron-sized HAp particles were investigated as biomaterials for bone regeneration [15–17]. Nanofibers are attractive materials for bone tissue engineering due to their extremely large surface areas and similarities to natural extracellular matrix (ECM) [18]. However, traditional electrospinning method generally results in two dimensional (2D) fibrous matrices, which limit cellular infiltration. A number of recent studies show that, three dimensional (3D) fibrous matrices have larger pore sizes and higher porosity due to loosely packed fibres [19–21]. As a result, cells can proliferate through the depth of the scaffold and a more homogeneous cell distribution is observed when compared with 2D fibrous scaffolds. Many methods have been developed for 3D fibrous matrix fabrication via electrospinning including layer-by-layer electrospinning [22], post-processing [23], particulate leaching [24], collector modification [19], surfactant addition [20] and wet electrospinning. Among them, wet electrospinning is a simple and effective method for 3D fibrous matrix fabrication. In this method, a liquid bath is used as a collector instead of traditional 2D metal surfaces [21].

Recently, we have fabricated PBAT scaffolds by using conventional scaffold fabrication methods such as electrospinning, solvent casting-particulate leaching and melt moulding-particulate leaching [25]. Due to the highly porous nature, wettability properties and ECM similarity, 2D electrospun PBAT matrices supported viability and proliferation of MC3T3-E1 cells. However, novel approaches are necessary to mimic 3D and nanocomposite structure of native bone. To the best of our knowledge, this is the first study investigating the combination of amorphous B-HAp nanoparticles and ECM mimetic 3D electrospun PBAT scaffolds in terms of osteogenic differentiation of human bone marrow derived mesenchymal stem cells (hBMSCs). For this purpose, HAp and B-HAp containing 3D PBAT scaffolds were fabricated via wet electrospinning method. These nanofibrous scaffolds were characterized by SEM, TEM and their water absorption capacities and degradation behaviours were evaluated by gravimetric analyses. Then, *in vitro* proliferation and bone forming abilities of hBMSCs on 3D PBAT scaffolds were assessed by DNA analysis, SEM, ALP activity, calcium and collagen assays and RT-PCR.

## Materials and methods

### Materials

PBAT pellets were kindly supplied from SASA laboratories, Turkey. The molar compositions and sequence lengths of repeating units, BT (aromatic) and BA (aliphatic), were calculated via  $^{13}\text{C}$  NMR spectrum as 42% and 58%, respectively. Compositions were close to the commercial product of BASF with trade name Ecoflex<sup>®</sup> (BT: 44%, BA: 56%). Also, the average sequence lengths of PBAT were calculated as 2.56 for BA and 1.78 for BT, with a degree of randomness equal to 0.95.

For preparation of synthetic body fluid (SBF) and B containing SBF solutions, sodium chloride (NaCl), magnesium chloride hexahydrate ( $\text{MgCl}_2 \cdot 6\text{H}_2\text{O}$ ), calcium chloride dihydrate ( $\text{CaCl}_2 \cdot 2\text{H}_2\text{O}$ ), sodium dihydrogen phosphate monohydrate ( $\text{NaH}_2\text{PO}_4 \cdot \text{H}_2\text{O}$ ), sodium hydrogen carbonate ( $\text{NaHCO}_3$ ), sodium hydroxide (NaOH) and boric acid ( $\text{H}_3\text{BO}_3$ ) were purchased from Merck (Germany). Solvent, 1,1,1,3,3,3-hexafluoro-2-propanol (HFIP), was supplied from Merck. For cell culture studies, Minimum Essential Medium- $\alpha$  modification ( $\alpha$ -MEM) was purchased from Biochrom (Holliston, MA, USA). L-Glutamine, penicillin-streptomycin solution, foetal bovine serum (FBS), trypsin-EDTA and phosphate buffered saline (PBS) were supplied from Biowest (Nuaille, France). Ascorbic acid, dexamethasone, hexamethyldisilazane (HMDS) and  $\beta$ -glycerophosphate were supplied from Sigma-Aldrich (Germany).

### Preparation of HAp and B-HAp nanoparticles

For preparation of the ten times concentrated SBF ( $10 \times$  SBF-like) solution the recipe developed in our previous study [10] was applied. In brief, respectively 58.443 g NaCl, 0.373 g KCl, 3.675 g  $\text{CaCl}_2 \cdot 2\text{H}_2\text{O}$ , 1.016 g  $\text{MgCl}_2 \cdot 6\text{H}_2\text{O}$  and 0.250 g  $\text{NaH}_2\text{PO}_4 \cdot \text{H}_2\text{O}$  were dissolved in 900 ml of distilled water under stirring. Then, the volume of the solution was completed to 1000 mL with deionized water. About 84 mg

$\text{NaHCO}_3$  was added to solution prior to HAp precipitation from SBF solution. Finally, 600 W of microwave radiation (Milestone, Italy) was applied to the resultant solution for nine times, each for 30 s. Then suspension was centrifuged and washed two times with ethanol and three times with distilled water in order to remove impurities. The powders were left to dry overnight in an incubator. In case of B-HAp preparation, 10 g boric acid was dissolved in 1 L distilled water prior to salt addition. In order to adjust pH value of solution between 6.5 and 7.4, 10 M NaOH was added into the solution. After that, HAp synthesis procedure mentioned above was repeated for B-HAp synthesis.

### Fabrication of 3D PBAT, HAp-PBAT and B-HAp-PBAT fibrous matrices

Wet electrospinning method was used for fabrication of PBAT-based 3D fibrous matrices. For fabrication of neat PBAT fibres, PBAT (24% w/v) was dissolved in HFIP and stirred overnight. In order to produce HAp-PBAT or B-HAp-PBAT fibres, previously fabricated HAp or B-HAp powders were added into electrospinning solution with the ratio of 5% (w/w, with respect to polymer amount) and stirred overnight. Solution was transferred into syringe with 21-gauge needle and syringe was placed into syringe pump (NE 300; New Era Pump Systems, Farmingdale, NY, USA). High voltage (Gamma High Voltage Research, Ormond Beach, FL, USA) was applied between syringe and collector. Three-D samples were collected in ethanol bath for 2.5 h, with 21 kV of voltage, 0.6 mL/h of flow rate and 25 cm of distance between syringe tip and collector. After the spinning process, samples were washed with distilled water and freeze-dried for 48 h. The 3D PBAT composite matrices were in the size of the collector that was used (Petri dish with 5 cm diameter) and they were cut out with punch to 8.0 mm in diameter and 2.0 mm in thickness.

### Preparation of 2D PBAT matrices

Two-dimensional PBAT matrices were also fabricated by traditional electrospinning for comparison based on our previous study [25]. PBAT was first dissolved in HFIP at a concentration of 24% (w/v) and transferred into a syringe with a 21-gauge needle. Syringe was placed into a syringe pump and high voltage was applied between the needle and stationary collector. Fibres were collected on the flat metal collector for 2.5 h and fibrous matrices were obtained with approximately 400  $\mu\text{m}$  thickness at 21 kV of voltage, 1 mL/h of flow rate and 20 cm distance between collector and syringe tip. After spinning process, samples were dried under vacuum for 48 h.

### Characterization of fibrous matrices

Morphologies of fibrous matrices were investigated with scanning electron microscope (SEM) (Zeiss Evo 50, Oberkochen, Germany). All the samples were visualized after sputter coating with a thin layer of gold under vacuum (K550X Sputter Coater; Electron Microscopy Sciences, Hatfield, PA, USA). Pore sizes and fibre diameters were calculated

using ImageJ software (National Institutes of Health, MD, USA).

Morphologies of HAp and B-HAp particles embedded into PBAT fibres were investigated with transmission electron microscope (TEM) (FEI Tecnai G2 Spirit BioTwin CTEM, USA). Fibres were deposited on holey carbon grids for 15 s prior to analysis.

For the determination of equilibrium water content (EWC), water uptake studies were carried out in PBS (pH 7.4, 37 °C). Samples were immersed into PBS and removed within determined time intervals for gravimetric measurements. The percentage of EWC was determined by Equation (1):

$$\text{EWC (\%)} = [(W_w - W_d)/W_d] \times 100 \quad (1)$$

where  $W_d$  and  $W_w$  indicate the weight of dry and wet (at equilibrium) samples, respectively.

Porosities of samples were determined by gravimetric method Equation (2):

$$\text{Porosity (\%)} = [1 - (\rho_a/\rho_m)] \times 100 \quad (2)$$

where  $\rho_m$  is the density of PBAT (1.26 g/cm<sup>3</sup>). Apparent density ( $\rho_a$ ) was calculated by dividing the weight of sample by its volume.

Degradation of PBAT fibrous matrices was investigated both in enzymatic and non-enzymatic medium. For enzymatic degradation studies, each sample was soaked in 2 mL of PBS (pH 7.4, 37 °C) containing 1 mg lipase. Non-enzymatic degradation was carried out in the absence of lipase enzyme. Samples were taken from degradation medium and dried under vacuum for gravimetric analysis on the first, third and fifth weeks of assay. Weight loss of the samples was measured with triplicates. Degradation media of the samples were refreshed once a week.

## Cell culture studies

### Cell seeding

Cell culture studies were carried out with hBMSCs. Human bone marrow aspirate was obtained from Lonza (Allendale, NJ, USA), isolated and characterized as previously described [28]. Cells were cultured in flasks by using  $\alpha$ -MEM containing 10% (v/v) FBS and 1% (v/v) penicillin–streptomycin solution and kept in humidified CO<sub>2</sub> incubator (Panasonic, Osaka, Japan) at 37 °C. Prior to cell seeding, cells were dissociated with 0.25% trypsin-EDTA solution and suspended in growth medium. PBAT-based fibrous matrices were cut into disks, each with a diameter of 8 mm and thickness of 2 mm. Samples were sterilized in 70% ethanol for 1 h and then, under UV light for 30 min. After sterilization, the samples were conditioned with  $\alpha$ -MEM containing 10% FBS for 24 h. Ten  $\mu$ L of cell suspension was seeded into materials in order to provide inoculation densities of  $7 \times 10^4$  cells per scaffold. The cells were conducted in CO<sub>2</sub> incubator to permit adhesion for 3 h and 10  $\mu$ L of growth medium was added to each sample in every 30 min to keep samples wet. After all, 1 mL of growth medium was added to each well and one day after cell seeding, 100 nM dexamethasone, 10 mM  $\beta$ -glycerophosphate and 0.05 mM ascorbic acid were added into the medium to stimulate osteogenic differentiation. During the

culture studies, cells were incubated in humidified CO<sub>2</sub> atmosphere at 37 °C.

### Cell proliferation analysis

Proliferation of hBMSCs was analysed quantitatively with DNA analysis kit (Quant-iT™ PicoGreen™) on the 1st, 7th, 14th and 28th days of the culture. In order to prepare DNA extracts, 600  $\mu$ L of Triton X-100 solution was added to each sample and vortexed. The amounts of DNA were calculated from fluorescence intensities, which were read by fluorescence microplate reader (Molecular Devices, San Jose, CA, USA) with excitation and emission wavelengths of 480 nm and 520 nm, respectively.

### SEM analysis

Morphologies of hBMSCs were investigated with SEM on the 7th and 28th days of the culture. Scaffolds were first gently washed twice with PBS (0.01 M phosphate buffer, 0.0027 M potassium chloride and 0.137 M sodium chloride, pH 7.4) and cells were fixed with 2.5% glutaraldehyde in PBS at 4 °C for 30 min. Samples were thoroughly washed with PBS after fixation and kept in PBS at 4 °C until the SEM visualization. Before the analysis, scaffolds were dehydrated with ethanol series at different concentrations (30, 50, 70, 90 and 100% v/v) and dried with HMDS overnight. Finally, each sample was visualized after sputter coating with a thin layer of gold under vacuum (K550X Sputter Coater; Electron Microscopy Sciences, Hatfield, PA, USA) before SEM analysis.

### Cell differentiation analyses

*Determination of alkaline phosphatase (ALP) activity, collagen and calcium amounts via colorimetric assays.* For collagen assay, the scaffolds were first transferred into sterile Eppendorf tubes and they were homogenized in 100  $\mu$ L distilled water. Then, 100  $\mu$ L of 12 N HCl was added to each Eppendorf tube and hydrolysis was carried out at 120 °C for 3 h. For calcium analysis, calcium was extracted by using 5% (w/v) trichloroacetic acid under sonication for 30 min. Amounts of ALP, collagen and calcium were determined via colorimetric assay kits (Biovision, Milpitas, CA, USA) using the supernatants obtained as mentioned above. All assays were carried out by following the instructions of the assay kits. In brief, ALP activity was determined due to hydrolysis of p-nitrophenyl phosphate (pNPP) to p-nitrophenol (pNP). UV absorbance of pNP was read via microplate reader (ASYS, Hitech UVM 340 plate reader, UK) at 405 nm. Collagen amount in the ECM was directly proportional to hydroxyproline amount and it was determined via measuring the absorbance of hydroxyproline at 560 nm. Finally, calcium amounts were determined by measuring the absorbance of calcium–cresolphthalein complex at 575 nm. Samples without cells were used as negative controls for ALP, collagen and calcium assays and their absorbances were subtracted from each sample containing cells. ALP activities, collagen and calcium amounts were normalized to ng of DNA. The mineral formation on the scaffolds was also supported by an energy-dispersive X-ray spectroscopy (energy dispersive X-ray

**Table 1.** The primer sequences for hBMSCs used in this study.

Genes	Primers	
β-Actin	Forward	5'-GTGCTATGTTGCCCTAGACTTCG-3'
	Reverse	5'-GATGCCACAGGATCCATACCC-3'
Collagen-I (COL-I)	Forward	5'-CAAGATGTGCCACTCTGACT-3'
	Reverse	5'-TCTGACCTGTCTCCATGTTG-3'
Alkaline phosphatase (ALP)	Forward	5'-GAGCGACACGGACAAGAAG-3'
	Reverse	5'-TGGTAGTTGTTGTGACATAATC-3'
Osteocalcin (OCN)	Forward	5'-CTTCTGCTCACTCTGCTG-3'
	Reverse	5'-TATTGCCCTCTGCTTGG-3'
Osteopontin (OPN)	Forward	5'-CACTTCACTCCAATCGTCCCTAC-3'
	Reverse	5'-ACTCCTTAGACTCACCGCTCTTC-3'

[EDX], Xflash 3001 SDD-EDS detector) analysis attached to the SEM.

**Real time-reverse transcriptase polymerase chain reaction (RT-PCR) analysis.** Transcription levels of osteoblast specific genes (ALP, COL-I, OCN and OPN) were quantified via RT-PCR analysis (Light Cycler<sup>®</sup> Nano, Roche, Switzerland) and Quantitech, Sybergreen RT-PCR kit (Qiagen, Manchester, UK). Before the analysis, mRNA was isolated from the samples using Trizol reagent. Reverse transcription for cDNA synthesis was carried out at 40 °C for 120 min. PCR reaction was kept for 45 cycles at 95 °C for 15 min as the first activation step, then the second step with extension at 95 °C for 15 s, 60 °C for 20 s, 72 °C for 20 s and separation step at 60 °C for 4 s and 95 °C for 20 s. β-actin was used as a housekeeping gene and primer sequences were given in Table 1. Comparative CT method (the  $2^{-\Delta\Delta CT}$  method) was used to calculate the relative gene expressions.

### Statistical analysis

At least three parallel samples were used for all the analyses. Data were analysed using GraphPad Instat<sup>®</sup> software (GraphPad, San Diego, CA, USA). One-way ANOVA was used to determine the significant differences among the groups and a statistical significance was assigned as \* $p < .05$ , \*\* $p < .01$  and \*\*\* $p < .001$ , respectively.

## Results

### Fabrication of HAp and B-HAp particles

HAp and B-HAp nanoparticles were fabricated via microwave-assisted biomimetic precipitation method prior to electrospinning process. With respect to the previous studies of our group, synthesized HAp and B-HAp particles have amorphous structure with a Ca/P ratio of 1.61 and 1.40, respectively [10,14]. B-HAp particles precipitated from 10 mg/mL boric acid solution by 600 W microwave power have  $1.15 \pm 0.11\%$  (w/w) boron and  $4.30 \pm 0.07\%$  (w/w) carbonate content whereas HAp particles have carbonate content of  $7.15 \pm 0.28\%$  (w/w) [14]. TEM images of HAp and B-HAp particles were shown in Figure S1(a) and (b), respectively. HAp and B-HAp particles formed by nanocrystals with an approximate size of 30–50 nm and the resultants particles were in the size range of 200–400 nm [10,14]. These apatites resemble to the biological apatite found in bone with the morphology and amorphous structure.

## Characterization of PBAT-based 3D fibrous matrices

### Morphological analysis

PBAT, HAp-PBAT and B-HAp-PBAT fibrous matrices with thicknesses of 2.0 mm were fabricated successfully via wet electrospinning and characterized via SEM and TEM (Figure 1).

As seen from Figure 1, all fabricated PBAT-based fibres have smooth and bead-free morphology. Nevertheless, addition of HAp and B-HAp particles brought partially rough morphology to the PBAT fibres. HAp and B-HAp particles were dispersed into the fibrous matrices as well as embedded into the fibres (Figure 1(b,c)). HAp and B-HAp particles embedded into the fibres can be clearly seen from the TEM images of the fibres (Figure 1(h,i)) each with a size of approximately 1 μm. Although microwave-assisted biomimetic precipitation method [14] allows formation of HAp particles with the size of 40–50 nm, HAp particles probably agglomerated during stirring of the solution or during electrospinning process resulting in micron-sized particles.

According to Table 2, diameters of PBAT and B-HAp-PBAT fibres are approximately same whereas diameters of HAp-PBAT fibres are quite lower than those of PBAT and B-HAp-PBAT fibres. According to the histograms in Figure 1, more than 90% of the fibres are in the diameter ranges of 400–1400 nm for PBAT, 300–1200 nm for HAp-PBAT and 400–1500 nm for B-HAp-PBAT even though their average diameters are  $898 \pm 328$ ,  $614 \pm 289$  and  $899 \pm 351$  nm, respectively.

Characteristics of PBAT, HAp-PBAT and B-HAp-PBAT fibrous matrices are given in Table 2. In order to make a comparison between 2D and 3D fibrous matrices, characteristics of 2D PBAT fibrous matrices fabricated in our previous study [25] are also presented in Table 2. As seen from this table, porosity of the 2D fibrous matrices is ~86% whereas that of 3D fibrous matrices is ~91%. Moreover, pore sizes were also enhanced with the fabrication of 3D matrix as expected. It is important to consider that in wet electrospinning fibres are deposited with less density leading to the formation of loosely packed fibres with higher porosity and larger pore size. Differences of porosity and pore sizes between 2D and 3D fibrous matrices can be seen morphologically from Figure 2.

### Water uptake study

Water uptake studies show that, PBAT fibrous matrices that have HAp and B-HAp have higher equilibrium water content when compared with neat PBAT fibres (Table 2) (Figure S1). Since addition of HAp enhances wettability of the hydrophobic matrices [26], HAp containing fibrous matrices could absorb higher amount of water. However, no statistically significant difference was observed among the equilibrium water contents of 3D samples. Additionally, 3D samples had higher equilibrium water content when compared with 2D samples because of their higher pore size and porosity. All of the samples reached the equilibrium water content within few minutes due to their highly porous and flexible structure.

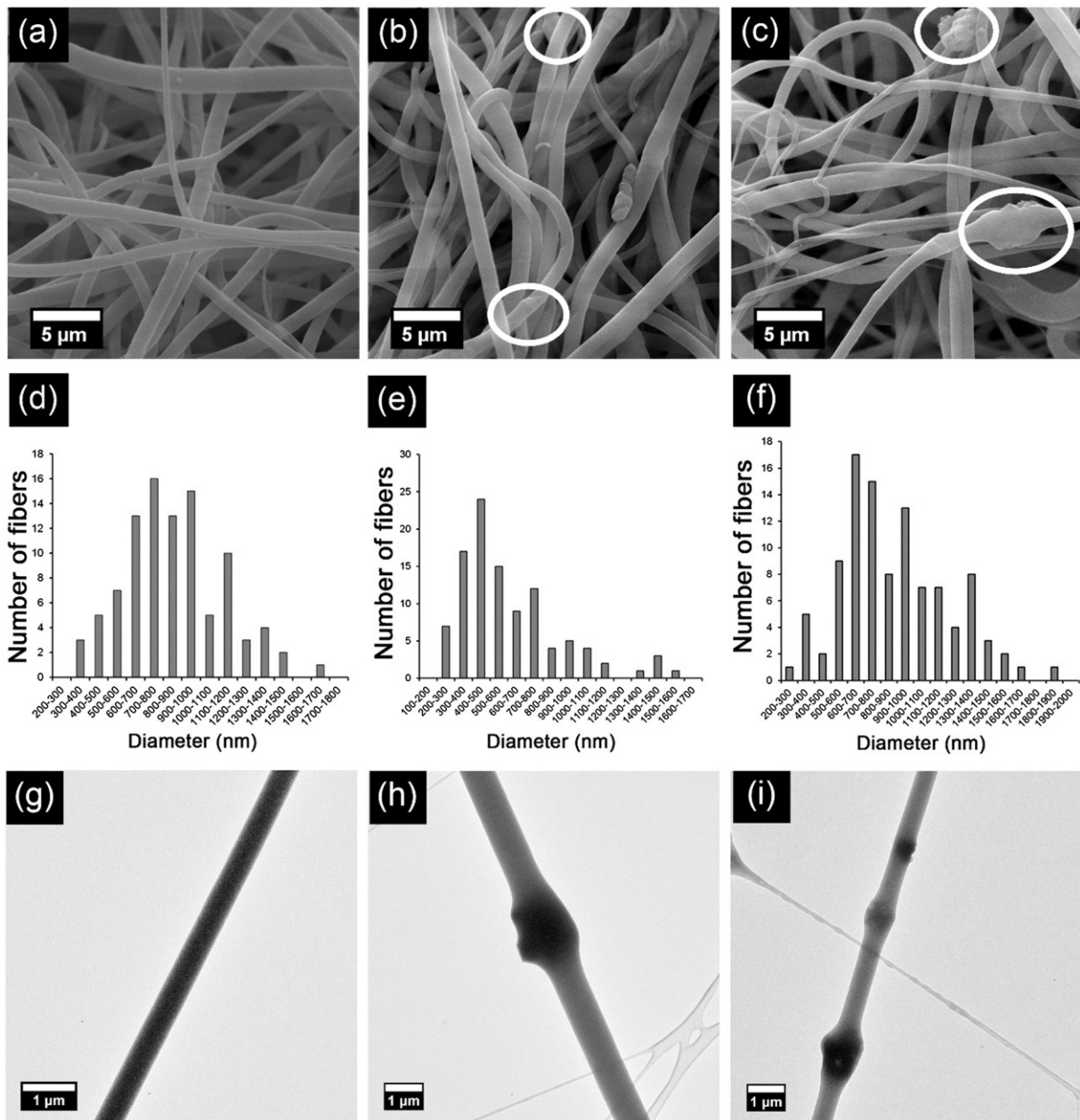


**Figure 1.** (a–c) SEM images, (d–f) histograms and (g–i) TEM images of (a, d, g) PBAT, (b, e, h) HAp-PBAT and (c, f, i) B-HAp-PBAT fibres. White circles indicate HAp and B-HAp particles dispersed in fibrous mats.

**Table 2.** Characteristics of 2D and 3D PBAT fibrous matrices.

Form	Fibres	Average fibre diameter (nm)	Pore size ( $\mu\text{m}$ )	Porosity (%)	Equilibrium water contents (%)
2D	PBAT	$569 \pm 187$	$12 \pm 4$	$85.6 \pm 3.7$	$475 \pm 42$
3D	PBAT	$898 \pm 328$	$30 \pm 22$	$91.2 \pm 0.6$	$515 \pm 59$
	HAp-PBAT	$614 \pm 289$	$32 \pm 12$		$587 \pm 57$
	B-HAp-PBAT	$899 \pm 351$	$25 \pm 7$		$563 \pm 40$

### Degradation study

In this study, we carried out degradation experiments in the presence of lipase enzyme and the results were evaluated in terms of weight changes during 5 week of incubation period. According to the results of degradation assay (Figure S2), weight of the enzymatically degraded samples decreased approximately by 10% at the end of the fifth week, whereas that of non-enzymatically degraded samples was limited with 3%.

### Cell culture studies

#### DNA analysis and SEM imaging

In order to determine DNA amounts of the cells proliferated on 3D PBAT matrices quantitative DNA analysis was performed on the 1st, 7th 14th and 28th days of the culture and the results were given in the Figure 3. At the first day of the culture, no statistically significant difference was observed among DNA amounts of PBAT, HAp-PBAT and B-HAp-PBAT

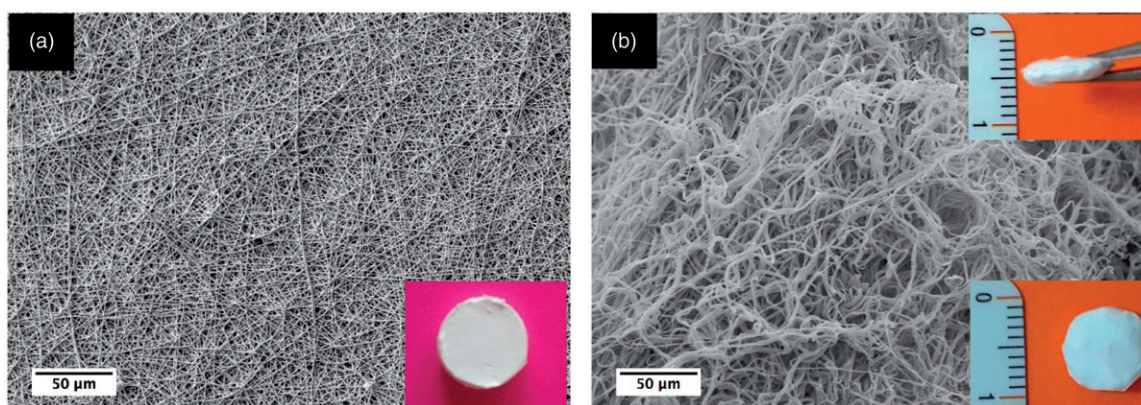


**Figure 2.** Comparison of 2D and 3D PBAT fibrous scaffolds: (a) 2D and (b) 3D PBAT fibrous matrices (Magnitudes: 1000 $\times$ ). Inset images show gross views of 2D and 3D electrospun matrices.

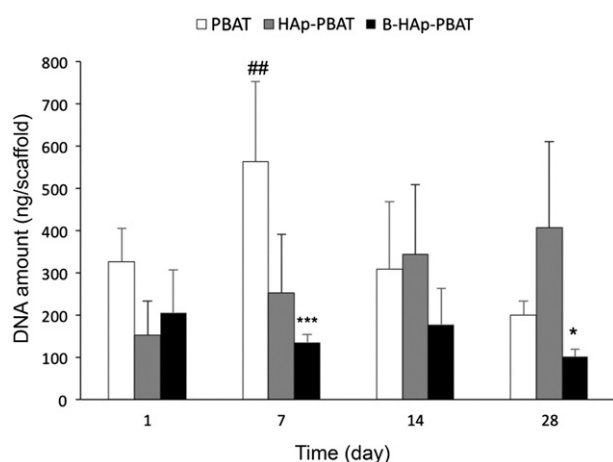


**Figure 3.** Proliferation of hBMSCs on PBAT, HAp-PBAT and B-HAp-PBAT scaffolds based on DNA analysis. Statistically significant differences; \* $p < .05$ , \*\* $p < .01$ , \*\*\* $p < .001$ ,  $n = 3$ .

scaffolds. However, at the 7th day of the culture, DNA amount of hBMSCs cultured on PBAT and HAp-PBAT scaffolds increased while that of B-HAp-PBAT fibres remained constant. Besides, DNA amounts of the cells cultured on PBAT scaffolds were significantly higher than the other groups. At the 14th and 28th days of the culture, DNA amounts of the cells on PBAT scaffolds decreased whereas that of HAp-PBAT scaffolds increased and B-HAp-PBAT scaffolds remain constant. These results are consistent with SEM analysis as shown in Figure 4(a–c) that cells completely covered the surface of the PBAT scaffolds. Morphologies of the cells on PBAT based scaffolds at the 7th and 28th days of the culture can be seen in Figure 4 and indicated that PBAT based scaffolds promoted the cell attachment and proliferation.

As can be seen from Figure 5(a–c), increases of ALP activity, collagen and calcium amounts on PBAT scaffolds between 14 and 28 days confirmed that hBMSCs were in the matrix maturation and differentiation phase. After HAp incorporation into PBAT scaffolds, cell proliferation continuously increased throughout the culture period. This result suggests that HAp-PBAT scaffolds supported the long term proliferation of hBMSCs with respect to neat PBAT. Comparing the cell proliferation on PBAT and HAp-PBAT scaffolds with B-HAp-PBAT,

the presence of B-HAp resulted low level of cell proliferation during the whole culture period.

At the 28th day, ECM mineralization can be clearly observed from the inset SEM images on Figure 4(d–f). Mineral nodules produced by cells showed typical apatite morphology as observed on inset images. The size of mineral nodules observed on PBAT scaffolds was bigger than the nodules on HAp-PBAT and B-HAp-PBAT scaffolds. However, nodules on B-HAp-PBAT scaffolds showed the highest density with respect to other groups. At the EDX analysis, the formation of Ca and P peaks proved the mineral formation on PBAT, HAp-PBAT and B-HAp-PBAT scaffolds (Figure 4(g–i)). Spherical morphology of the particles seen in inset images of Figure 4(d–f) and the presence of Ca, P and O peaks on EDX spectra proved that the particles were the biological HAp synthesized by differentiated hBMSCs. As a result, the peaks observed at 1.040 and 2.620 keV belong to the sodium and chloride elements which was most probably reasoned by the PBS used in washing steps for sample preparation before SEM analysis.

### Cell differentiation

Amounts of ALP, calcium and collagen formed in the matrices are presented in Figure 5. ALP activity of hBMSCs cultured on PBAT and B-HAp-PBAT scaffolds increased until the 28th day of the culture whereas that of HAp-PBAT scaffolds remained constant (Figure 5(a)). ALP activity of the hBMSCs on HAp-PBAT scaffolds were significantly higher than that of cells on PBAT scaffolds at day 7 ( $p < .01$ ). At the 28th day of the culture, ALP activity level of hBMSCs cultured on B-HAp-PBAT scaffolds was significantly higher than that of the other groups ( $p < .001$ ). ALP activity of hBMSCs continuously increased on B-HAp-PBAT scaffolds during 4 weeks of osteogenic culture (Figure 5(a)), as a result, the incorporation of B into the amorphous HAp improved the osteogenic differentiation of hBMSCs throughout the culture period. Due to the fact that a continuous increase of DNA amount on HAp-PBAT scaffolds during the culture, a significant DNA amount decrease for PBAT scaffolds after day 7 and the lowest DNA amount seen on B-HAp-PBAT scaffolds throughout the culture confirmed why the highest ALP activity observed on B-HAp-PBAT scaffolds. Collagen amounts of the scaffolds remained constant until the 14th day of the culture (Figure 5(b)). At the

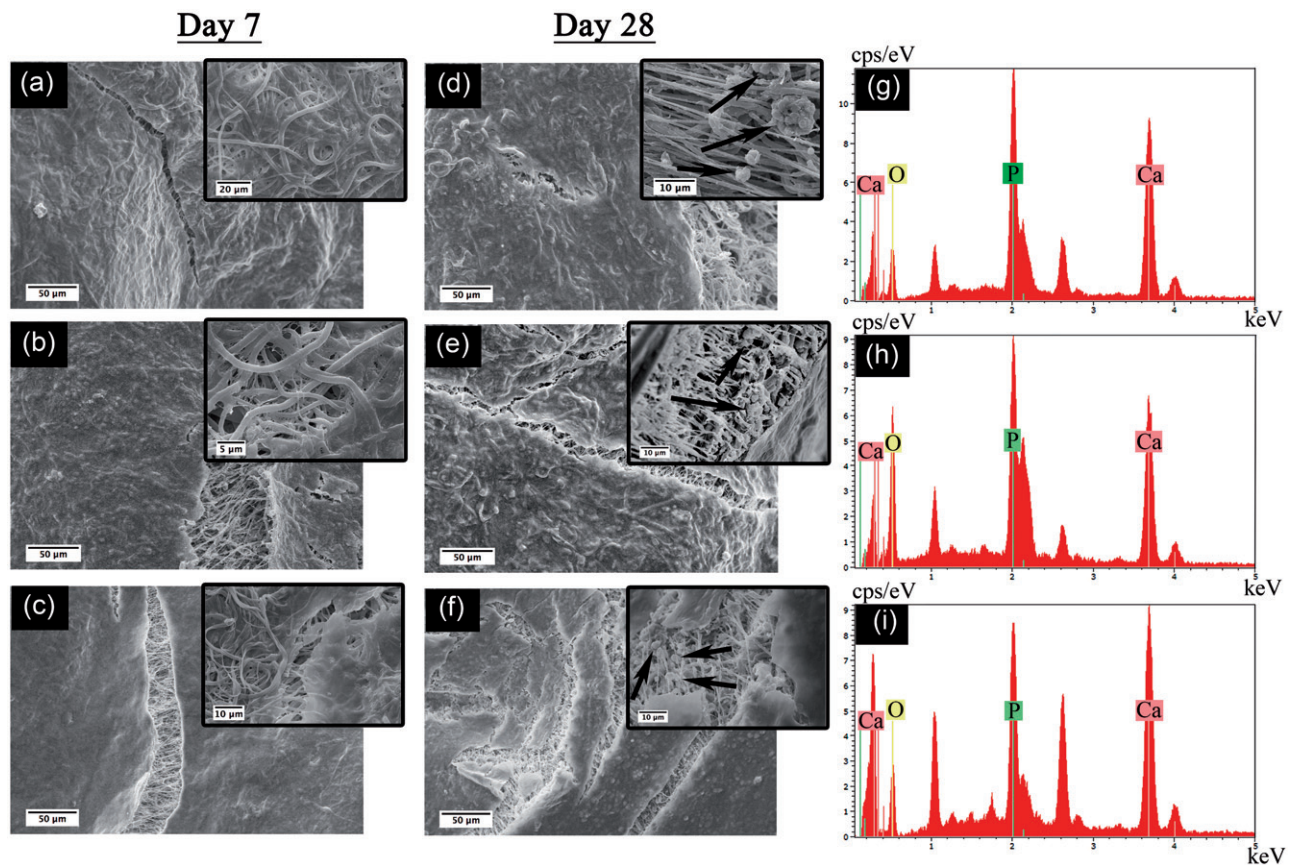


**Figure 4.** SEM images of hBMSCs cultured on PBAT-based scaffolds: (a, d) PBAT, (b, e) HAp-PBAT and (c, f) B-HAp-PBAT scaffolds. Left column corresponds to the day 7 SEM images whereas middle column shows the SEM images at day 28. (g), (h) and (i) images show EDS spectra of mineralized areas on PBAT, HAp-PBAT and B-HAp-PBAT scaffolds for the samples at day 28, respectively.

28th day of the culture, collagen amount of B-HAp-PBAT scaffolds increased to a level that was significantly higher than those of PBAT and HAp-PBAT scaffolds ( $p < .05$  and  $p < .01$ ).

Calcium amounts of all scaffolds were increased at the 28th day of the culture as expected (Figure 5(c)). However, the highest calcium amount was detected in the B-HAp-PBAT scaffolds.

The remarkable effect of boron-doped HAp on osteogenic differentiation of hBMSCs was also proved with RT-PCR analyses. ALP, collagen I (COL-I), osteocalcin (OCN) and osteopontin (OPN) relative gene expressions were presented in Figure 6.

Relative ALP gene expressions were found similar with the spectrophotometric ALP assay (Figure 6(a)). ALP expressions of hBMSCs cultured on PBAT and B-HAp-PBAT scaffolds increased at the 28th day of the culture whereas those of HAp-PBAT scaffolds remained constant. The relative ALP gene expression at the B-HAp-PBAT scaffolds is approximately 2.5 times higher than that of PBAT scaffolds and seven times higher than that of HAp-PBAT scaffolds ( $p < .01$  and  $p < .001$ ).

Similarly, COL-I gene expressions of hBMSCs cultured on PBAT and HAp-PBAT scaffolds remained constant for the 14th day of the culture (Figure 6(b)). COL-I expressions of the cells cultured on PBAT and HAp-PBAT scaffolds increased slightly at the 28th day. However, COL-I expression of hBMSCs in B-HAp-PBAT scaffolds was 12 and 16 times higher than those

of PBAT and HAp-PBAT scaffolds at the 28th day of the culture, respectively ( $p < .01$ ).

Expressions of the mineralization regulating genes, OCN and OPN, can be seen on Figure 6(c,d). OCN and OPN gene expressions remained constant until the 14th day of culture whereas they increased at the 28th day. Similarly, gene expressions were remarkably higher in case of B-HAp-PBAT scaffolds at the 28th day of culture ( $p < .001$ ).

## Discussion

Although PBAT is a co-polyester, it is comprised of both aliphatic and aromatic units. Interestingly, aromatic segments of PBAT has been also shown to be enzymatically cleaved in presence of mixed microbial populations [27]. However, it has been reported that amount of the aromatic units as well as their sequence length is a critical factor affecting the degradation rate of PBAT. Witt and co-workers reported that PBAT degrades faster when amount and sequence of the aromatic units are less than 55% and 3%, respectively [28]. Based on the NMR studies done in our previous study, aromatic content of the PBAT is found as 42% where the average sequence length of the butylene terephthalate units is equal to 1.78 [25]. In the present study, we have observed weight loss in the 3D fibre matrices after incubation in enzymatic medium for five weeks, which can be considered as an indication of degradation in the *in vivo* conditions. Weight loss of the 3D PBAT fibrous matrices in this study corresponds with



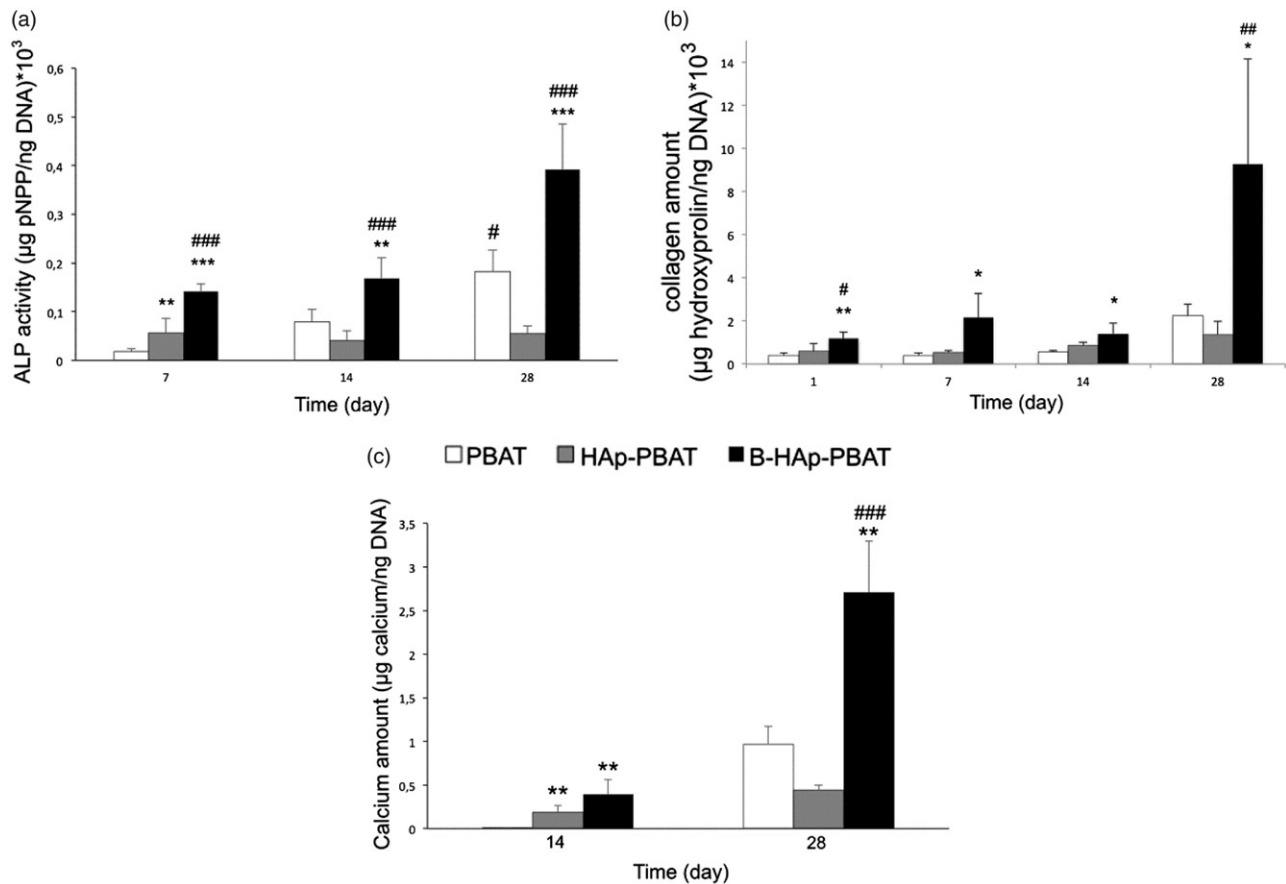


**Figure 5.** Osteoblastic differentiation of hBMSCs cultured on PBAT-based scaffolds based on colorimetric assays: (a) ALP activity, (b) calcium and (c) collagen amounts. Statistically significant differences; \* $p < 0.05$ , \*\* $p < 0.01$ , \*\*\* $p < 0.001$  when control group is PBAT scaffold and # $p < 0.05$ , ## $p < 0.01$ , ### $p < 0.001$  when control group is HAp-PBAT scaffold,  $n = 3$ .

the weight loss profile of PBAT scaffolds with similar porosity in our previous study [25].

Besides inducing osteoinductive properties, HAp also act as a buffer in the medium due to its basic resorption products, which helps minimizing the negative effect of acidic degradation products of polyesters on the cell functions [29]. Among various HAp synthesis techniques, microwave assisted precipitation technique has been preferred to synthesize bone-like HAp in a fast, simple and efficient way. Via the use of microwave for precipitation of HAp, the Gibbs free energy is reduced and the intermediate steps are avoided, which results in the synthesis of pure, bone-like HAp with narrow size distribution in shorter mineralization times compared to the other methods [10]. Recently, our group determined optimum conditions of bone-like HAp synthesis via microwave-assisted precipitation of 10xSBF-like solution. The resulting HAp showed similar properties to those of cortical bone [10].

Recently, osteoinductive effect of HAPs have been further enhanced via doping boron, which has been known as a critical trace element in human body and playing an important role in bone metabolism. Gümüşderelioğlu et al. [30] examined the effects of encapsulated boron on proliferation and differentiation of MC3T3-E1 pre-osteoblastic cells *in vitro* and reported that it has a stimulatory effect on osteoblasts. Fabrication of boron-doped HAp (B-HAp) via biomimetic method was investigated in our research group for the first

time, where B-HAp is applied as a coating on chitosan scaffolds via microwave-assisted precipitation of concentrated SBF containing boron [14]. The results showed that boron has improved the osteoinductive and osteoconductive impact of HAp on differentiation of hBMSCs, indicated with enhanced OCN, OPN and COL-I expressions. In the present study, we investigated the effect of B-HAp fabricated via biomimetic method on osteogenic differentiation of hBMSCs in form of particles incorporated into electrospun fibres, to create uniform distribution of B-HAp over the bulk electrospun scaffold. As expected, the scaffolds containing boron-doped HAp has shown the most significant impact on osteogenic differentiation of hBMSCs.

*In vitro* bone formation involves proliferation, matrix maturation and mineralization stages. Cell proliferation is followed by the synthesis of COL-I, which is the most abundant protein of bone, and an increase in the ALP gene expression and activity. In the beginning of mineralization, non-collagenous proteins such as OCN and OPN are deposited in the matrix [31,32]. Theoretically, COL-I and ALP expressions raise on early differentiation states. However, in our study, the highest expression levels were recorded in late differentiation states. This effect might be a result of late release of ions from entrapped HAp and B-HAp, which delays the expressions of COL-I and ALP. Moreover, agglomeration of the HAp and B-HAp particles during electrospinning process

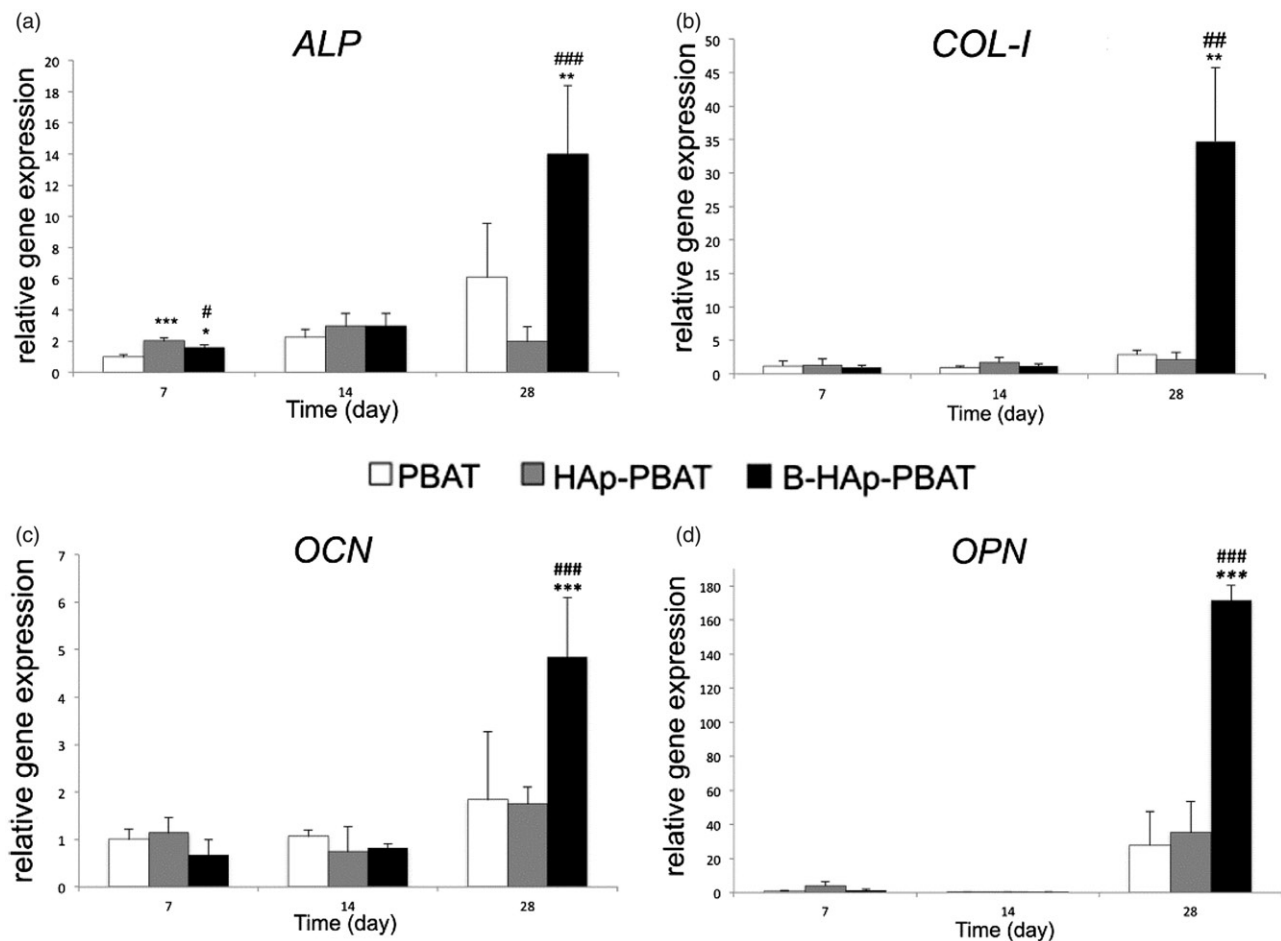


**Figure 6.** Osteoblastic differentiation of hBMSCs cultured on PBAT based scaffolds: (a) ALP activity, (b) collagen 1 (COL 1), (c) osteocalcin (OCN) and (d) osteopontin (OPN) gene expressions, based on real-time PCR analysis. Statistically significant differences; \* $p < 0.05$ , \*\* $p < 0.01$ , \*\*\* $p < 0.001$  when control group is PBAT scaffold and # $p < 0.05$ , ## $p < 0.01$ , ### $p < 0.001$  when control group is HAp-PBAT scaffold,  $n = 3$ .

might have decreased the active surface area of HAp and B-HAp, which might have decreased the release rate of the ions and thus delayed the expressions.

According to the Barheine et al. [33], *in vitro* degradation of B-HAp was faster than that of HAp or  $\beta$ -TCP. Therefore, we can conclude that local increase of boron concentration due to the faster degradation of B-HAp triggered cells to osteoblastic differentiation rather than proliferation as also confirmed by the ALP analysis, calcium amount and detection of the osteogenic differentiation markers via RT-PCR analyses. The higher expressions of OCN and OPN of hBMSCs in the B-HAp-PBAT scaffolds indicate that addition of B induces the mineralization remarkably. After all, it was observed that hBMSCs cultured on B-HAp-PBAT scaffolds had the highest level of ALP activity, calcium and collagen amounts throughout the culture period.

## Conclusions

In the presented study, PBAT fibrous matrices were fabricated via wet electrospinning and biomimetic HAp and B-HAp particles were added into the fibrous matrices. Bioactivities of the scaffolds were investigated via proliferation and differentiation of hBMSCs. According to SEM and TEM analysis, PBAT fibres have smooth and bead-free morphology and HAp and

B-HAp particles were both dispersed in matrix and embedded into the fibres. When compared with 2D matrices, wet electrospun 3D matrices have pore sizes approximately three times higher than that of 2D fibrous matrices. PBAT based scaffolds promoted attachment and proliferation of hBMSCs according to SEM and quantitative DNA analysis. All PBAT based scaffolds supported proliferation and differentiation of the cells. However, differentiation of the cells were not affected significantly with addition of HAp particles to PBAT fibres whereas B-HAp particles strongly enhanced the differentiation process. Regarding to these results, it can be concluded that wet electrospun PBAT fibrous scaffolds are estimated to be a good alternative for bone regeneration, especially after modification with boron doped HAp.

## Acknowledgement

The authors are grateful to Selin Gümüşderelioğlu for editing the language of the text.

## Disclosure statement

No potential conflict of interest was reported by the authors.

## References

- [1] Costa-Pinto AR, Salgado AJ, Correlo VM, et al. Adhesion, proliferation, and osteogenic differentiation of a mouse mesenchymal stem cell line (BMC9) seeded on novel melt-based chitosan/polyester 3D porous scaffolds. *Tissue Eng Part A*. 2008;14:1049–1057.
- [2] Fukushima K, Rasyida A, Yang MC. Characterization, degradation and biocompatibility of PBAT based nanocomposites. *Appl Clay Sci*. 2013;80–81:291–298.
- [3] Jao WC, Lin CH, Hsieh JY, et al. Effect of immobilization of polysaccharides on the biocompatibility of poly(butylene adipate-co-terephthalate) films. *Polym Adv Technol*. 2010;21:543–553.
- [4] Nar M, Staufenberg G, Yang B, et al. Osteoconductive bio-based meshes based on Poly(hydroxybutyrate-co-hydroxyvalerate) and poly(butylene adipate-co-terephthalate) blends. *Mater Sci Eng C*. 2014;38:315–324.
- [5] Wang A, Gan Y, Yu H, et al. Improvement of the cytocompatibility of electrospun poly[(R)-3-hydroxybutyrate-co-(R)-3-hydroxyvalerate] mats by Ecoflex. *J Biomed Mater Res A*. 2012;100:1505–1511.
- [6] Santana-Melo GF, Rodrigues BVM, da Silva E, et al. Electrospun ultrathin PBAT/nHAP fibers influenced the *in vitro* and *in vivo* osteogenesis and improved the mechanical properties of neoformed bone. *Colloids Surf B Biointerfaces*. 2017;155:544–552.
- [7] Asgari F, Samiei M, Adibkia K, et al. Biodegradable and biocompatible polymers for tissue engineering application: a review. *Artif Cells Nanomed Biotechnol*. 2017;45:185–192.
- [8] Chen F-M, Liu X. Advancing biomaterials of human origin for tissue engineering. *Prog Polym Sci*. 2016;53:86–168.
- [9] Mavis B, Demirtaş TT, Gümüşderelioğlu M, et al. Synthesis, characterization and osteoblastic activity of polycaprolactone nanofibers coated with biomimetic calcium phosphate. *Acta Biomater*. 2009;5:3098–3111.
- [10] Tolga Demirtaş T, Kaynak G, Gümüşderelioğlu M. Bone-like hydroxyapatite precipitated from 10 × SBF-like solution by microwave irradiation. *Mater Sci Eng C*. 2015;49:713–719.
- [11] Tohamy KM, Mabrouk M, Soliman IE, et al. Novel alginate/hydroxyethyl cellulose/hydroxyapatite composite scaffold for bone regeneration: *in vitro* cell viability and proliferation of human mesenchymal stem cells. *Int J Biol Macromol*. 2018;112:448–460.
- [12] Akram M, Ahmed R, Shakir I, et al. Extracting hydroxyapatite and its precursors from natural resources. *J Mater Sci*. 2014;49:1461–1475.
- [13] Hakki SS, Bozkurt BS, Hakki EE. Boron regulates mineralized tissue-associated proteins in osteoblasts (MC3T3-E1). *J Trace Elem Med Biol*. 2010;24:243–250.
- [14] Tunçay EÖ, Demirtaş TT, Gümüşderelioğlu M. Microwave-induced production of boron-doped HAp (B-HAp) and B-HAp coated composite scaffolds. *J Trace Elem Med Biol*. 2017;40:72–81.
- [15] Kim H-W, Lee H-H, Knowles JC. Electrospinning biomedical nanocomposite fibers of hydroxyapatite/poly(lactic acid) for bone regeneration. *J Biomed Mater Res*. 2006;79A:643–649.
- [16] Venugopal J, Low S, Choon AT, et al. Electrospun-modified nanofibrous scaffolds for the mineralization of osteoblast cells. *J Biomed Mater Res*. 2008;85A:408–417.
- [17] Lao L, Wang Y, Zhu Y, et al. Poly(lactide-co-glycolide)/hydroxyapatite nanofibrous scaffolds fabricated by electrospinning for bone tissue engineering. *J Mater Sci: Mater Med*. 2011;22:1873–1884.
- [18] Mohammadian F, Abhari A, Nejati-Koski K, et al. New state of nanofibers in regenerative medicine. *Artif Cells Nanomed Biotechnol*. 2017;45:204–210.
- [19] Blakeney BA, Tambralli A, Anderson JM, et al. Cell infiltration and growth in a low density, uncompressed three-dimensional electrospun nanofibrous scaffold. *Biomaterials*. 2011;32:1583–1590.
- [20] Cai S, Xu H, Jiang Q, et al. Novel 3d electrospun scaffolds with fibers oriented randomly and evenly in three dimensions to closely mimic the unique architectures of extracellular matrices in soft tissues: fabrication and mechanism study. *Langmuir*. 2013;29:2311–2318.
- [21] Ki CS, Kim JW, Hyun JH, et al. Electrospun three-dimensional silk fibroin nanofibrous scaffold. *J Appl Polym Sci*. 2007;106:3922–3928.
- [22] Levorson EJ, Sreerekha PR, Chennazhi KP, et al. Fabrication and characterization of multiscale electrospun scaffolds for cartilage regeneration. *Biomed Mater*. 2013;8:14103.
- [23] Wright LD, Young RT, Andric T, et al. Fabrication and mechanical characterization of 3D electrospun scaffolds for tissue engineering. *Biomed Mater*. 2010;5:55006.
- [24] Kim TG, Chung HJ, Park TG. Macroporous and nanofibrous hyaluronic acid/collagen hybrid scaffold fabricated by concurrent electrospinning and deposition/leaching of salt particles. *Acta Biomater*. 2008;4:1611–1619.
- [25] Arslan A, Çakmak S, Cengiz A, et al. Poly(butylene adipate-co-terephthalate) scaffolds: processing, structural characteristics and cellular responses. *J Biomater Sci Polym Ed*. 2016;27:1841–1859.
- [26] Tihan TG, Ionita MD, Popescu RG, et al. Effect of hydrophilic–hydrophobic balance on biocompatibility of poly(methyl methacrylate) (PMMA)–hydroxyapatite (HA) composites. *Mater Chem Phys*. 2009;118:265–269.
- [27] Witt U, Einig T, Yamamoto M, et al. Biodegradation of aliphatic-aromatic copolyesters: evaluation of the final biodegradability and ecotoxicological impact of degradation intermediates. *Chemosphere*. 2001;44:289–299.
- [28] Witt U, Müller R-J, Deckwer W-D. Studies on sequence distribution of aliphatic/aromatic copolyesters by high-resolution <sup>13</sup>C nuclear magnetic resonance spectroscopy for evaluation of biodegradability. *Macromol Chem Phys*. 1996;197:1525–1535.
- [29] Huttmacher DW. Scaffolds in tissue engineering bone and cartilage. *Biomaterials*. 2000;21:2529–2543.
- [30] Gümüşderelioğlu M, Tunçay EÖ, Kaynak G, et al. Encapsulated boron as an osteoinductive agent for bone scaffolds. *J Trace Elem Med Biol*. 2015;31:120–128.
- [31] Beck GR. Inorganic phosphate as a signaling molecule in osteoblast differentiation. *J Cell Biochem*. 2003;90:234–243.
- [32] Lian JB, Stein GS. Concepts of osteoblast growth and differentiation: basis for modulation of bone cell development and tissue formation. *Crit Rev Oral Biol Med*. 1992;3:269–305.
- [33] Barheine S, Hayakawa S, Jäger C, et al. Effect of disordered structure of boron-containing calcium phosphates on their *in vitro* biodegradability. *J Am Ceram Soc*. 2011;94:2656–2662.